

magnitude in this parameter does not alter our conclusion that cells typically maintain free copper at insignificant concentrations. The upper limit for $[Cu(I)]_{free}$ calculated in the same manner as for $Cu(II)$, is estimated to be less than 10^{-23} M. To obtain this value, we used the known $Cu(I)/Cu(II)$ reduction potentials of CuSOD (400 mV) and aqueous $Cu(II)$ (153 mV) in a thermodynamic cycle with the K_1' of Eq. 1 to obtain an equilibrium constant for $Cu(I)$ binding to SOD (2×10^{20}). The equilibrium $[Cu(I)]_{free}$ would be five orders of magnitude lower than estimates for $Cu(II)$.

22. A less reliable kinetic model yields a range of intracellular $[Cu]_{free}$ values for the *lys7* null strain data in Table 1. Assumptions include a second-order rate law $d[CuSOD]/dt = k_1 [apo-SOD][Cu]_{free}$ where $[apo-SOD] \sim 10 \mu M$ (moles of total SOD1 per volume of a cell), t is time, and k_1 is the second-order rate constant. The rate $d[CuSOD]/dt < 3 \times 10^{-8}$ M per 60 hours is about $10^{-13} M s^{-1}$, where 60 hours corresponds to the typical lifetime of a yeast cell with a doubling time of ≥ 2 hours and a life-span of no more than 30 divisions [D. A. Sinclair, K. Mills, L. Guarente, *Trends Biochem. Sci.* **23**, 131 (1998)]. The volume accessible to ySOD and copper

ions is assumed to be about 1/4 of the total volume of a yeast cell, where the latter is 7×10^{-14} liters [F. Sherman, in *Methods in Enzymology*, C. Guthrie and G. R. Fink, Eds. (Academic Press, Orlando, FL, 1991), vol. 194, pp. 3–21]. Two limiting conditions for k_1 were considered. If the rate for copper binding to ySOD1 is diffusion controlled ($k_1 = 10^8 M^{-1} s^{-1}$), the upper limit of $[Cu]_{free}$ is 10^{-16} M. When a lower limit for k_1 of $10^4 M^{-1} s^{-1}$ was used, $[Cu]_{free}$ is $< 10^{-12}$ M. This lower limit for k_1 was obtained by measuring the increase in active ySOD1 concentration (by cytochrome *c* assay) after incubation of $Cu(II)$ with apo-ySOD1 for 5 to 60 s. Metal insertion was quenched by EDTA (1 mM), which prevents further loading of apo-ySOD1.

23. V. C. Culotta et al., *J. Biol. Chem.* **270**, 29991 (1995).
 24. D. R. Rosen et al., *Nature* **362**, 59 (1993).
 25. H.-X. Deng et al., *Science* **261**, 1047 (1993).
 26. S.-J. Lin and V. C. Culotta, *Mol. Cell. Biol.* **16**, 6303 (1996).
 27. F. Sherman et al., *Methods in Yeast Genetics* (Cold Spring Harbor Laboratory Press, Cold Spring Harbor, NY, 1978).
 28. L. Flohe and F. Otting, in *Methods in Enzymology*, L.

- Packer, S. P. Colowick, N. O. Kaplan, Eds. (Academic Press, Orlando, FL, 1984), vol. 105, pp. 93–104.
 29. S. A. Goscin and I. Fridovich, *Biochim. Biophys. Acta* **289**, 276 (1972).
 30. J. Hirose, T. Ohhira, H. Hirata, Y. Kidani, *Arch. Biochem. Biophys.* **218**, 179 (1982).
 31. T. J. Lyons et al., *J. Biol. Inorg. Chem.* **3**, 650 (1998).
 32. We thank D. Hamer for yeast strain 19.3C; J. Valentine for the ySOD1-pET3d plasmid; D. Kosman for yeast SOD1 antibody; I. Klotz, J. Widom, and D. Huffman for advice; and J. Strain, A. Torres, and A. Herrreiter for technical assistance. Supported in part by NIH grants GM 54111 (T.V.O.), GM 50016 (V.C.C.), F32 GM19457 (T.D.R.), and F32 DK09305 (R.A.P.); National Institute of Environmental Health Science training grant ES07141 (P.J.S.); the Johns Hopkins University National Institute for Environmental Health Science Center (V.C.C.); and the Amyotrophic Lateral Sclerosis Association (T.V.O.). T.V.O. is a member of the Robert H. Lurie Comprehensive Cancer Center.

28 December 1998; accepted 18 March 1999

Effects of Angiogenesis Inhibitors on Multistage Carcinogenesis in Mice

Gabriele Bergers,¹ Kashi Javaherian,² Kin-Ming Lo,³ Judah Folkman,² Douglas Hanahan^{1*}

Solid tumors depend on angiogenesis for their growth. In a transgenic mouse model of pancreatic islet cell carcinogenesis (RIP1-Tag2), an angiogenic switch occurs in premalignant lesions, and angiogenesis persists during progression to expansive solid tumors and invasive carcinomas. RIP1-Tag2 mice were treated so as to compare the effects of four angiogenesis inhibitors at three distinct stages of disease progression. AGM-1470, angiostatin, BB-94, and endostatin each produced distinct efficacy profiles in trials aimed at preventing the angiogenic switch in premalignant lesions, intervening in the rapid expansion of small tumors, or inducing the regression of large end-stage cancers. Thus, anti-angiogenic drugs may prove most efficacious when they are targeted to specific stages of cancer.

Over the past decade, genetically engineered mouse models of cancer have increasingly been used in studies on mechanisms of carcinogenesis. One strength of these models is that cancers arise from normal cells in their natural tissue microenvironments and progress through multiple stages, as does human cancer (1). Such models of organ-specific cancer also present opportunities for development not only of cancer therapies but also of preventative strategies that block the progression of premalignant lesions into tumors.

The RIP1-Tag2 transgenic mouse model

of pancreatic islet carcinogenesis serves as a general prototype of the pathways, parameters, and molecular mechanisms of multistage tumorigenesis. The pathway through which normal insulin-producing β cells of the pancreatic islets are converted into islet cell carcinomas under the influence of the SV40 T antigen (Tag) is increasingly well understood (2, 3). Briefly, in the RIP1-Tag2 line, the following stages arise sequentially over the 13.5-week average lifetime of these mice. Normal islets (initially 100% of the ~ 400 islets per pancreas) express the Tag oncogene and yet are morphologically asymptomatic until 3 to 4 weeks of age. Hyperplastic islets then begin to appear stochastically (increasing to 50% of the islets by 10 weeks), displaying β -cell hyperproliferation and features of dysplasia and carcinoma in situ. Angiogenic islets (8 to 12%) arise from hyperplastic/dysplastic islets by switching on angiogenesis in the normally quiescent islet capillaries (3). This switch is characterized by

endothelial proliferation, vascular dilation, and microhemorrhaging. Solid tumors ($\sim 3\%$ of the islets) emerge at 10 weeks as small encapsulated tumors (adenomas) that progress by 12 to 13 weeks into large adenomas and (less frequently) invasive carcinomas, both of which are intensely vascularized by dilated hemorrhagic vessels.

In earlier work, we showed that a mixture of three angiogenesis inhibitors (AGM-1470, minocycline, and alpha interferon) could inhibit tumor growth in the RIP-Tag model (4). These data supported other preclinical data from subcutaneous transplant models (5–7). Encouraged by the result, we designed the present study to assess the effects of four diverse angiogenesis inhibitors when applied to RIP1-Tag2 mice at three distinct stages of pancreatic islet carcinogenesis. Figure 1 illustrates the experimental design, which had three branches: (i) early treatment at the hyperplastic stage to block the angiogenic switch before the initial formation of solid tumors (prevention trial), (ii) treatment of mice bearing small (asymptomatic) solid tumors to determine whether their expansive growth and progression to deleterious stages could be stopped (intervention trial), and (iii) treatment of mice with substantial tumor burden and near death to ascertain whether these agents could induce tumor regression (regression trial). We evaluated four angiogenesis inhibitors (8) (Tables 1 and 2): AGM-1470 (TNP470), BB-94 (batimastat), angiostatin, and endostatin, as well as the combination of angiostatin and endostatin. AGM-1470 (TNP470) is a small molecule inhibitor of endothelial cell proliferation (9) that is thought to act by inhibiting an intracellular enzyme, methionylaminopeptidase-2 (9). BB-94 (batimastat) is a broad-spectrum inhibitor of matrix metalloproteinases (10), which are involved in the remodeling of extracellular matrix and capillary basement membranes during angiogenesis (11). An-

¹Department of Biochemistry and Biophysics and Hormone Research Institute, University of California, San Francisco, 513 Parnassus Ave, San Francisco, CA 94143-0534, USA. ²Department of Surgery, Children's Hospital Medical Center and Harvard Medical School, 300 Longwood Avenue, Boston, MA 02115, USA. ³Lexigen Pharmaceuticals, 125 Hartwell Avenue, Lexington, MA 02173, USA.

*To whom correspondence should be addressed. E-mail: dh@biochem.ucsf.edu

REPORTS

giostatin and endostatin are cleavage products of larger cellular proteins. Angiostatin is an internal fragment of plasminogen, whereas endostatin is a COOH-terminal fragment of collagen XVIII, itself a component of the blood vessel wall (6, 7). In this study, we used murine versions of angiostatin and endostatin that were produced as fusions to the Fc fragment of the murine immunoglobulin heavy chain (Tables 1 and 2) (12).

In the prevention trial, 5-week-old transgenic mice harboring only hyperplastic nonangiogenic islets were treated for 5.5 weeks, to the point at which tumors first began to appear in sham-treated controls (Table 1) (13). At this age (10.5 weeks), 20 to 25% of the hyperplastic islet nodules (~45 islets) had become angiogenic (3), which allowed the frequency of the angiogenic switch to be quantitated before tumor burden grossly disrupted the pancreatic architecture. AGM-1470 had no statistically significant effect, and angiostatin had only a modest impact on the number of angiogenic islets, as compared to saline treatment. In contrast, BB94 reduced the incidence of angiogenic switching by ~50%, whereas endostatin alone and the combination of endostatin plus angiostatin resulted in 61 and 63% reductions, respectively.

In the intervention trial, treatment of the RIP1-Tag2 mice began at 10 weeks of age, when every mouse had a few small but highly vascularized solid tumors, and ended at 13.5 weeks, when sham-treated mice had end-stage disease (13). We assessed tumor burden rather than life-span extension, in order to fully evaluate the tumor size and histological characteristics such as apoptotic index and vessel density. As shown in Table 2, all four compounds were efficacious. Fc-angiostatin was least effective, reducing tumor burden by ~60%. AGM-1470, BB-94, and Fc-endostatin reduced tumor growth by 82, 83, and 88%, respectively. The Fc-angiostatin plus Fc-en-

dostatin combination was not tested here because of a limited supply of Fc-angiostatin.

In the regression trial, we treated cohorts of 12-week-old tumor-bearing mice that had a life expectancy of <2 weeks. We assessed life-span

extension as well as tumor burden. The control mice were moribund by 13.5 weeks and were killed. All of the angiogenesis inhibitors extended life-span by at least 2 weeks. Because a subset of mice in some of the treatment groups

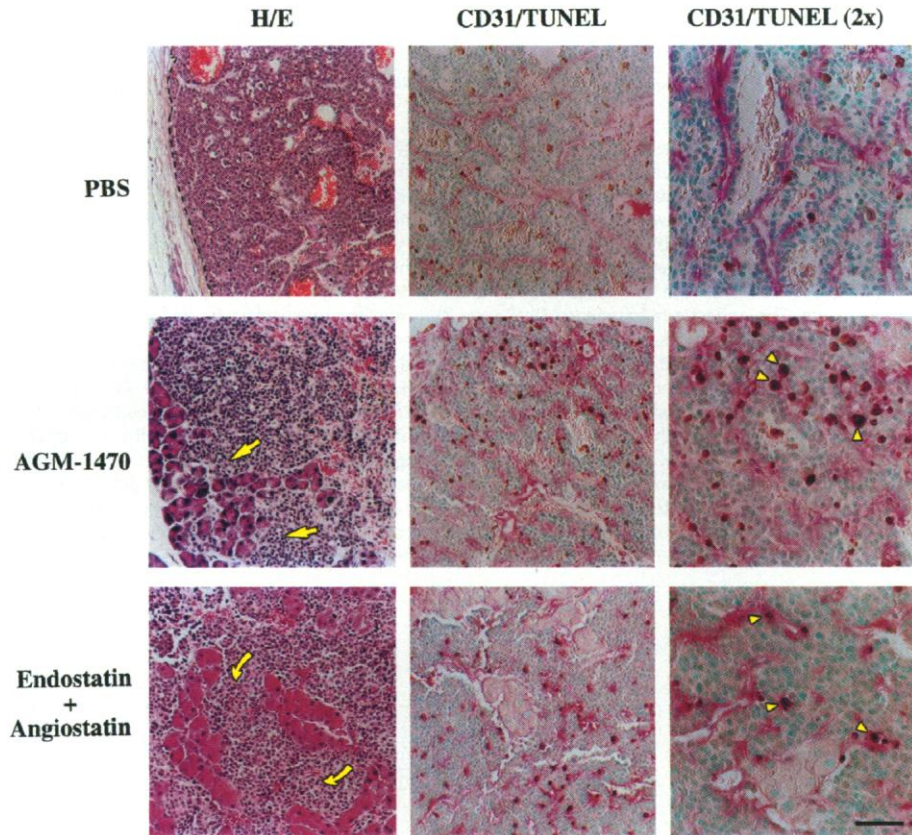
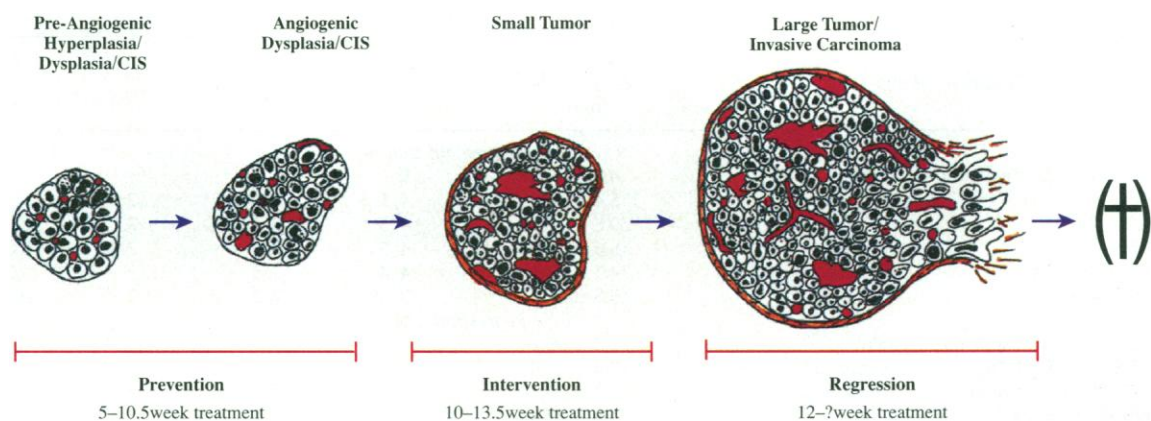


Fig. 2. Illustrative histopathology of the regression trial. Morphology [hematoxylin and eosin (H/E) staining] and combined endothelial and apoptotic cell labeling (anti-CD31+TUNEL) of tumors are shown. Tumor-bearing pancreases were collected from 13.5-week-old control RIP1-Tag2 mice and from 16-week-old transgenic mice treated with AGM-1470 or a combination of Fc-angiostatin and Fc-endostatin. Pancreases were then fixed, paraffin-embedded, and sectioned at 5 μm . Yellow arrows indicate the invasive fronts of carcinomas, and yellow arrowheads indicate apoptotic cells proximal to blood vessels. Scale bar indicates 44.6 μm in the H/E and CD31/TUNEL panels and 22.3 μm in the CD31/TUNEL (2 \times) panels.

Fig. 1. Anti-angiogenic trials designed to target discrete stages of carcinogenesis. The RIP1-Tag2 mice develop pancreatic insulinomas and islet cell carcinomas in a multi-step pathway that includes an angiogenic switch before solid tumor formation. In the prevention trials, inhibitors were tested for their ability to block a hallmark of tumor development: the onset of angiogenesis.

Thus, 5-week-old transgenic mice, whose islets had not yet activated the angiogenic switch, were treated until the first tumors appeared in control mice at 10.5 weeks of age. For intervention studies, designed to address whether angiogenesis inhibitors can slow or stop tumor growth, 10-week-old transgenics bearing small tumors were treated until end-stage



disease (13.5 weeks of age). In the regression trials, inhibitors were tested for their ability to extend life-span by inducing regression of large tumors. Thus, treatment was initiated in 12-week-old transgenics harboring substantial tumor burden and with a life expectancy of less than 2 weeks. Cross at right indicates the death of the animal.

REPORTS

were moribund at 16 weeks, the trial was terminated at that time to allow comparison of tumor burden and histological characteristics (Table 2 and Fig. 2). Both AGM1470 and the combination of Fc-angiostatin plus Fc-endostatin caused significant regression of tumor burden. In contrast, Fc-endostatin alone, Fc-angiostatin alone, and BB-94 alone only slowed tumor growth. At 16 weeks, the tumor burden of mice treated with these compounds was similar to that of sham-

treated mice at 13.5 weeks and was increased from the 12-week starting point. Thus, in the regression trial, significant differences in efficacy were observed among the tested compounds.

In all three trials, we performed histological analyses (14) to compare either premalignant lesions or tumors from treated and control mice. In the prevention trial, the angiogenic islets in treated mice did not show obvious histological differences from those in control mice, in terms

of vessel density, hemorrhage formation, apoptotic index, or morphological appearance (15). The treated tumors in the intervention and regression trials had several common characteristics, as noted previously (4, 16). Angiogenesis inhibitor treatment did not induce a significant change in the number of proliferating tumor cells, it caused only a slight reduction in vessel density, and it increased the number of apoptotic cells by a factor of 2 to 3. The histopathology of the regression trial is shown for AGM-1470 and the Fc-endostatin plus Fc-angiostatin combination (Fig. 2). The observation that blood vessel density was not decreased (Fig. 2) supports the notion that some tumor vessels can grow, or at least remain intact, in the face of treatment with angiogenesis inhibitors; these vessels apparently dictate the number of tumor cells that can survive, thus governing tumor size while maintaining a similar density of tumor vessels. Although it was not surprising that apoptosis was induced in endothelial cells treated with the anti-angiogenic compounds, it was intriguing that tumor cells in close apposition to capillaries were also frequently apoptotic. One might have expected the opposite: that oxygen and nutrient deprivation resulting from an impaired vasculature would preferentially affect hypoxic tumor cells most distal to capillaries; the periendothelial apoptotic pattern suggests that the apoptotic induction mechanism involves signals distinct from hypoxia.

There was an appreciable incidence (35 to 52%) of invasive islet cell carcinomas among the small tumors present at 16 weeks in all treatment groups (Fig. 2); they were most pronounced (52%) in mice treated with Fc-endostatin or Fc-angiostatin

Table 1. Prevention trial. The average number \pm SD of angiogenic islets of control (PBS) and treated mice and the reduction in the number of angiogenic islets (%) are shown. The reduction in angiogenic islet incidence in treated (T) versus control (C) mice was calculated by the formula $(1 - T/C) \times 100$. Statistical analysis was done with a two-tailed, unpaired Mann-Whitney test comparing experimental groups to (phosphate-buffered saline (PBS)-injected control mice. *P* values less than 0.1 are considered statistically significant. "N start" indicates the number of animals at the beginning of the trial; "N stop" indicates the number of animals at the end of the trial; and "N trials" indicates the number of independent experiments. The endostatin fragment of collagen XVIII and the angiostatin fragment of plasminogen were each fused at their respective NH₂-termini to the constant region of immunoglobulin G (Fc), the hybrid genes were expressed in murine myeloma cells, and the fusion proteins were isolated as described (12). BB-94 was homogenized in 0.02% Triton and PBS (pH 7.0) and given as an emulsion. AGM-1470 was dissolved in 5% dextrose water. Mice were treated with 25 mg per kilogram of body weight (25 mg/kg) of AGM-1470 s.c. every other day; or with 30 mg/kg of BB-94 i.p. every day; or with 15 mg/kg of Fc-endostatin s.c. every day, and/or with 20 mg/kg Fc-angiostatin s.c. every day. The dose of 15 mg/kg of Fc-endostatin was the maximal tolerable dose because of an inflammatory side effect produced by the fusion protein, which resulted in swollen faces and hair loss (or white hair on the head) but did not provoke an evident specific immune response in the form of T and B cell infiltration in the pancreas (15). Neither the Fc fragment alone nor endostatin without the Fc fragment elicited such allergic reactions.

Treatment group	Average number of angiogenic islets (\pm SD)	N start	N stop	N trials	<i>P</i> value	Reduction in angiogenic islets (%)
PBS control	46.0 \pm 6.7	5, 5	5, 5	2	—	0
AGM-1470	40.6 \pm 10.1	5, 5	5, 5	2	0.3641	11.7
BB-94	23.5 \pm 4.7	4, 4	3, 3	2	0.0014	48.9
Fc-endostatin	18.0 \pm 4.8	4, 5	3, 4	2	0.0008	60.9
Fc-angiostatin	33.8 \pm 5.2	6	6	1	0.0057	26.5
Fc-angiostatin + Fc-endostatin	17.0 \pm 4.6	5	5	1	0.0027	63.0

Table 2. The average tumor burden \pm SD of control (PBS) and treated animals and the reduction in tumor burden (%) in the treated animals are reported in the intervention and regression trial. The percent reduction in tumor burden was calculated from the average tumor burden of the treated groups (T) and the average tumor burden of the 13.5-week-old PBS-treated RIP1-Tag2 group by applying the formula $(1 - T/C) \times 100$. Statistical analysis was performed with a two-tailed, unpaired Mann-

Whitney test comparing experimental groups to PBS-injected control mice. *P* values less than 0.1 are considered statistically significant. Tumor burdens of experimental groups in the regression trial were compared to the tumor burden of 12-week-old Rip1-Tag2 animals. "N start" indicates the number of animals at the beginning of the trial; "N stop" indicates the number of animals at the end of the trial; and "N trials" indicates the number of independent experiments.

Treatment group	Average tumor burden (mm ³)	N start	N stop	N trials	<i>P</i> value	Reduction in tumor burden (%)
<i>Intervention trial</i>						
10-week Rip1-Tag2 starting point	4.2 \pm 0.54	5	—	—	—	0
13.5-week Rip1-Tag2 PBS control	115.4 \pm 43.0	4, 5, 5	3, 4, 3	3	—	0
AGM-1470	20.6 \pm 7.5	4, 5	3, 4	2	0.0008	82.2
BB-94	19.6 \pm 8.9	4, 5	3, 4	2	0.0008	83.0
Fc-endostatin	14.1 \pm 14.9	4, 4	3, 3	2	0.0014	87.8
Fc-angiostatin	46.5 \pm 21.8	3, 4	2, 3	2	0.0040	59.7
<i>Regression trial</i>						
12-week Rip1-Tag2 starting point	77.3 \pm 36.2	7	—	—	—	0
13.5-week Rip1-Tag2 control endpoint	115.4 \pm 43.0	—	10	—	—	0
AGM-1470 (16 weeks)	32.3 \pm 19.1	5, 6	4, 2*	2	0.0350	58.8
BB-94 (16 weeks)	114.3 \pm 53.9	5	4	1	0.4121	None
Fc-endostatin (16 weeks)	106.2 \pm 37.5	5	3	1	0.3833	None
Fc-angiostatin (16 weeks)	111.1 \pm 47.4	5	3	1	0.3833	None
Fc-angiostatin + Fc-endostatin (16 weeks)	31.8 \pm 11.5	7, 6	5†	2	0.0177	58.9

*Four mice were left in trial; three mice died at 17.7, 19.5, and 19.8 weeks of age; one mouse is still alive (20.2 weeks at 16 April 1999).

†Three mice were left in trial and died at 18, 19.5, and 20 weeks of age.

REPORTS

plus Fc-endostatin. In contrast, multiple large encapsulated adenomas predominated at the 12-week starting point of the regression trial, where only ~20% of tumors were invasive carcinomas. Thus, these angiogenesis inhibitors did not prevent histological progression to the invasive carcinoma stage. Metastases were not observed in the 16-week-old treated mice with prevalent carcinomas; however, metastasis is rare in control RIP1-Tag2 mice (2, 16).

Our data reveal that the four angiogenesis inhibitors tested had different efficacies depending on the stage of carcinogenesis being targeted (Fig. 3). BB-94, Fc-endostatin, the Fc-angiostatin plus Fc-endostatin combination, and to a lesser extent Fc-angiostatin, but not AGM-1470, prevented activation of the angiogenic switch in up to 63% in the hyperplastic islets that otherwise would have switched. Treatment of RIP1-Tag2 mice bearing substantial tumors with AGM-1470 or Fc-endostatin plus Fc-angiostatin produced significant tumor regression, in contrast to Fc-endostatin, Fc-angiostatin, or BB-94 alone. The former agents reduced tumor volume by ~60% (as compared to tumor volume at the 12-week starting point) and by ~72% (as compared to tumor burden in untreated mice near end stage

at 13.5 weeks). Given that the time course of each trial was limited, none of the agents tested completely prevented the angiogenic switch, blocked the growth of small tumors, or completely resolved lethal tumor burden. However, it is important to recognize that the *RIP1-Tag* transgene targets oncogene expression to every one of the ~500,000 pancreatic β cells in these transgenic mice, resulting in a temporal spectrum of developing neoplastic foci and thus rendering this a very stringent system for assaying pharmacological interventions. Although multifocal disease may present a tough standard in comparison to standard tumor transplant models, such stringency is likely to prove of considerable value, given the biological and clinical resilience of human cancers.

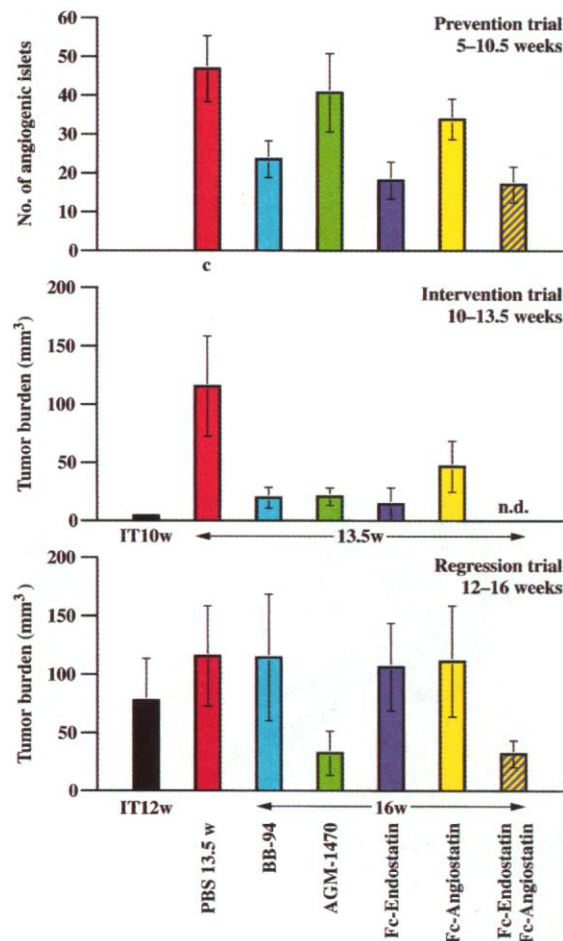
This study strengthens the proposition that angiogenesis inhibitors will become important components of anticancer treatment strategies, by using compounds and dosing regimens fine-tuned to target specific stages of disease progression. A number of future applications for this model system can be envisioned: identifying the most potent formulations, dosing regimens, and combinations of the current compounds as well as of new angiogenesis inhibitors, both for prevention and for therapeutics; exploring broader com-

binatorial possibilities involving other classes of anticancer drugs; and elucidating the pharmacogenetic mechanisms of the stage-specific efficacy differences. The challenge will be to validate the results from this and other mouse models of organ-specific carcinogenesis as instructive in the design of clinical trials to identify drugs and delivery strategies that are effective for the treatment and prevention of human cancers.

References and Notes

1. J. M. Adams and S. Cory, *Science* **254**, 1161 (1991); D. Hanahan, G. Christofori, P. Naik, J. Arbeit, *Eur. J. Cancer* **42A**, 2386 (1996); M. P. Rosenberg, *Mol. Carcinogen.* **20**, 262 (1997); S. D. Hursting, *Curr. Opin. Oncol.* **9**, 487 (1997).
2. D. Hanahan, *Nature* **315**, 115 (1985); J. Folkman, K. Watson, D. Ingber, D. Hanahan, *ibid.* **339**, 58 (1989); G. Bergers, D. Hanahan, L. M. Coussens, *Int. J. Dev. Biol.* **42**, 995 (1998); A.-K. Perl, P. Wilgenbus, U. Dahl, H. Semb, G. Christofori, *Nature* **392**, 190 (1998); J. H. Hager and D. Hanahan, in *Mechanisms of Cell Death*, Z. Zakeri, L. Benitez-Bribiesca, R. A. Lockshin, Eds. (New York Academy of Sciences, New York, in press).
3. J. Folkman, K. Watson, D. Ingber, D. Hanahan, *Nature* **339**, 58 (1989).
4. S. Parangi et al., *Proc. Natl. Acad. Sci. U.S.A.* **93**, 2002 (1996).
5. B. A. Teicher et al., *Int. J. Cancer* **57**, 920 (1994); B. A. Teicher, Y. Emi, Y. Kakeji, *Eur. J. Cancer* **32A**, 2461 (1996); P. Vajkoczy et al., *Neoplasia* **1**, 31 (1999).
6. M. S. O'Reilly et al., *Cell* **79**, 314 (1994); M. S. O'Reilly, L. Holmgren, C. Chen, J. Folkman, *Nature Med.* **2**, 689 (1996).
7. M. S. O'Reilly et al., *Cell* **88**, 277 (1997); T. Boehm, J. Folkman, T. Browder, M. S. O'Reilly, *Nature* **390**, 404 (1997).
8. The mice used in this study were males and females of the RIP1-Tag2 transgenic mouse lineage (2) inbred in the C57Bl/6J background. All control mice received subcutaneous (s.c.) or intraperitoneal (i.p.) saline injections. Subcutaneous injections were specifically directed to a region above the tail at the right or left flank known to be permissive for systemic delivery [R. Auerbach and W. Auerbach, *Science* **215**, 127 (1982)]. In the prevention trial, animals were treated from 5 to 10.5 weeks of age; in the intervention trial, from 10 to 13.5 weeks of age; and in the regression trial, from 12 to 16 weeks of age. All mice were maintained in accord with the University of California, San Francisco, institutional guidelines governing the care of laboratory mice and were killed after the respective treatment period.
9. D. Ingber et al., *Nature* **348**, 555 (1990); E. C. Griffith et al., *Chem. Biol.* **4**, 461 (1997); N. Sin et al., *Proc Natl. Acad. Sci. U.S.A.* **94**, 6099 (1997); V. Castronovo and D. Belotti, *Eur. J. Cancer* **32A**, 2520 (1996).
10. D. C. Talbot and P. D. Brown, *Eur. J. Cancer* **32A**, 2528 (1996).
11. Z. Werb, T. H. Vu, J. L. Rinkenberger, L. M. Coussens, in *Protease and Protease Inhibitors in Cancer Therapy*, L. Matrisian, N. Brunner, K. Dano, Eds. (*Acta Pathologica, Microbiologica, et Immunologica Scandinavica*, Human Press, Totowa, NJ, in press).
12. Additional information on the production and purification of murine angiostatin and endostatin as Fc fusion proteins is available at www.sciencemag.org/feature/data/990055.shl.
13. In the intervention and regression trials, animals were killed at the end of each trial, and tumors were microdissected from freshly excised pancreases. Tumor volume (in cubic millimeters) was measured with calipers, and the formula [volume = $0.52 \times (\text{width})^2 \times (\text{length})$] for approximating the volume of a spheroid was applied. Tumor burden per mouse was calculated by accumulating the tumor volumes of every mouse. In the prevention trial, angiogenic islets were isolated by retrograde perfusion with collagenase solution and counted. Angiogenic islets were identified as those that exhibited a reddish patch or patches (caused by hemorrhaging) in a white nodular

Fig. 3. Summary of stage-specific efficacy differences among angiogenic inhibitors. The relative effects of particular angiogenesis inhibitor treatments in the three distinct stages of carcinogenesis are compared here. IT stands for initial tumor burden at the beginning of the intervention trial (10 weeks; IT10w) or regression trial (12 weeks; IT12w). The prevention trial was started at 5 weeks of age, when only hyperplastic/dysplastic islet nodules are present (c in the top panel stands for the number of angiogenic islets in the control animals).



background (3). The visual scoring scheme has been confirmed by histology as described [S. Parangi *et al.*, *Cancer Res.* **55**, 66071 (1995)].

14. Microdissected tumors and pancreases were immersion-fixed in 4% paraformaldehyde and embedded in paraffin. Apoptotic index and vessel density were assessed by combined TUNEL [P. Naik *et al.*, *Genes Dev.* **10**, 2105 (1996)] and CD31 staining. Apoptotic labeling was followed by CD31 staining with a 1:100 dilution of a rat anti-mouse CD31 monoclonal antibody (Pharmingen). Reaction products were visualized with an ABC

kit, using as chromophores 3,3'-diaminobenzidine (for TUNEL-positive cells) and alkaline phosphatase substrate (for CD31 staining). Proliferating cells were detected with a mouse antibody against human proliferation-associated nuclear antigen (Biogenex). Ten to 20 fields of the respective sections were scored under oil immersion light microscopy.

15. G. Bergers, K. Javaherian, K.-M. Lo, J. Folkman, D. Hanahan, data not shown.
16. S. N. Grant, I. Seidman, D. Hanahan, *Cancer Res.* **51**, 4917 (1991).

17. We thank British Biotech Pharmaceuticals, Oxford, UK, for BB-94 and Takeda-Abbott Pharmaceuticals for AGM1470; S. Gillies of Letigan Pharmaceuticals for advice and support of the production of Fc-endostatin and Fc-angiostatin; E. Soliven for excellent technical assistance; A. McMillan for statistical analysis; and R. Weinberg, R. Klausner, J. M. Bishop, J. D. Watson, S. Parangi, J. Hager, E. Bergsland, and H. Ee for comments and critical reading of the manuscript. Supported by grants from the National Cancer Institute.

5 January 1999; accepted 30 March 1999

Unexpected Modes of PDZ Domain Scaffolding Revealed by Structure of nNOS-Syntrophin Complex

Brian J. Hillier,¹ Karen S. Christopherson,² Kenneth E. Prehoda,¹ David S. Brecht,² Wendell A. Lim^{1*}

The PDZ protein interaction domain of neuronal nitric oxide synthase (nNOS) can heterodimerize with the PDZ domains of postsynaptic density protein 95 and syntrophin through interactions that are not mediated by recognition of a typical carboxyl-terminal motif. The nNOS-syntrophin PDZ complex structure revealed that the domains interact in an unusual linear head-to-tail arrangement. The nNOS PDZ domain has two opposite interaction surfaces—one face has the canonical peptide binding groove, whereas the other has a β -hairpin "finger." This nNOS β finger docks in the syntrophin peptide binding groove, mimicking a peptide ligand, except that a sharp β turn replaces the normally required carboxyl terminus. This structure explains how PDZ domains can participate in diverse interaction modes to assemble protein networks.

PDZ protein interaction domains (1) play a central role in organizing diverse signaling pathways (2–7). The scaffolding protein InaD (inactivation no after potential), which comprises five PDZ domains, tethers multiple proteins of the *Drosophila* phototransduction cascade (6). The postsynaptic density protein PSD-95, which has three PDZ domains, clusters and localizes *N*-methyl-D-aspartic acid (NMDA)-type glutamate receptors at synapses (2). By organizing such protein networks, PDZ scaffolding proteins increase the efficiency and specificity of signal transduction.

Most known PDZ-mediated interactions occur through recognition of short COOH-terminal peptide motifs (2). Peptide interaction screens indicate that the terminal carboxylate of these ligands is required for binding (8). This canonical mode of PDZ recognition is well characterized: structures of PDZ-peptide complexes reveal that recognition is achieved through an extended binding groove

that terminates in a conserved carboxylate binding loop (9, 10).

Nonetheless, an increasing number of PDZ-mediated interactions occur through modes that are not dependent on recognition of a COOH-terminal motif. A well-characterized example is the PDZ domain of neuronal nitric oxide synthase (nNOS), the neuron- and muscle-specific isoform of the enzyme that produces the second

messenger nitric oxide (NO). The PDZ domain of nNOS specifically heterodimerizes with PDZ domains from PSD-95 and syntrophin in neurons and muscle cells, respectively (5). These interactions allow the integration of nNOS into specific signaling pathways. Association with PSD-95 in neurons is thought to couple NO production to NMDA receptor activation (11). Association with syntrophin in muscle cells localizes nNOS to the dystrophin complex (12), coupling NO production to muscle contraction. The resulting NO exerts a protective effect by increasing blood flow to match the heightened metabolic load of contracting muscle. Loss of this response in Duchenne muscular dystrophy may contribute to muscle degeneration (13).

These PDZ-PDZ interactions are distinct from canonical PDZ-peptide interactions in that they do not involve recognition of a COOH-terminal sequence on either partner protein. Moreover, the full tertiary structures of both PDZ partners are required, including 30 amino acids in nNOS that extend beyond the canonical PDZ region (5). These interactions are representative of an alternative class of PDZ domain interactions: the recognition of internal motifs. Such internal interactions have also been reported for PDZ domains from the scaffolding proteins GRIP and InaD (7, 14).

We determined the crystal structures of the nNOS PDZ domain alone and in complex with the syntrophin PDZ domain to 1.25 and 1.9 Å resolution, respectively (15) (Table 1).

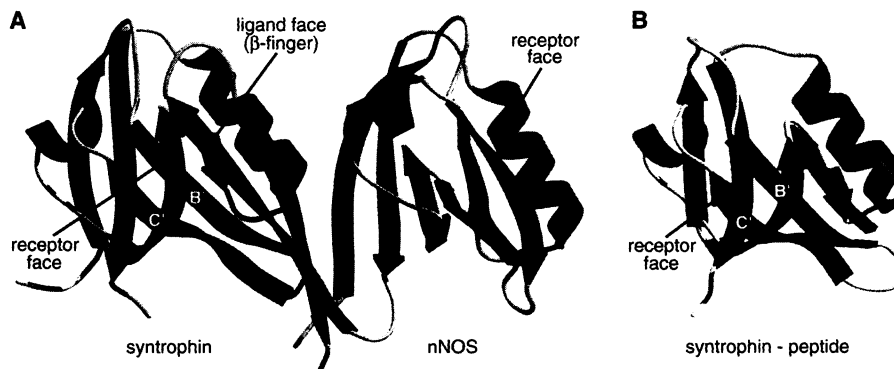


Fig. 1. Linear head-to-tail heterodimer of nNOS-syntrophin PDZ domains. (A) The nNOS PDZ domain (orange) has a polarized structure with distinct receptor (peptide binding groove) and ligand (β -finger) faces. The nNOS ligand face docks against the syntrophin PDZ domain (purple) peptide binding groove. (B) Structure of the syntrophin PDZ domain (purple) in complex with a COOH-terminal peptide (orange) (10). The figure was generated with the program MOLSCRIPT (25).

¹Department of Cellular and Molecular Pharmacology and Department of Biochemistry and Biophysics, ²Department of Physiology, University of California, San Francisco, San Francisco, CA 94143, USA.

*To whom correspondence should be addressed. E-mail: wlim@itsa.ucsf.edu